A numerical study of free-surface turbulence in channel flow

Y. Pan and S. Banerjee[a)]
Department of Chemical and Nuclear Engineering, University of California, Santa Barbara, California 93106

(Received 29 September 1994; accepted 13 March 1995)

Direct numerical simulations of open-channel flow indicate that turbulence at the free surface contains large-scale persistent structures. They are "upwellings" caused by impingement of bursts emanating from the bottom boundary; "downdrafts" in regions where adjacent upwellings interact, and whirlpool-like "attached vortices" which form at the edge of upwellings. The attached vortices are particularly long-lived in the sense that once formed, unless destroyed by other upwellings, they tend to interact with each other and dissipate only slowly. If turbulence generation at the bottom wall is turned off by changing the boundary condition to free slip, then the upwellings (related to bursts) and downdrafts no longer form. The dominant structures at the free surface become the attached vortices which pair, merge, and slowly dissipate. In the central regions, as expected, the structure remains three dimensional throughout the decay process. Near the free surface, the structure appears to be quasi- two dimensional, as indicated by quantitative measures such as energy spectra, interwave number energy transfer, invariants of the anisotropy tensor, and length scales. In the decaying case, the quasi-two-dimensional region increases in thickness, with decay time, though the structure in the central regions of the flow remains three dimensional. © *1995 American Institute of Physics.*

I. INTRODUCTION

Free-surface turbulence has a number of important applications. For example, interactions between the atmosphere and the ocean are strongly influenced by the structure of turbulence at the interface. Similarly, the persistent signatures of vessel wakes also appear to be influenced by free-surface turbulence.

Due to difficulties in measurement and simulation, very little was understood about the structure of turbulence near interfaces till recently. Experiments were first reported by Komori *et al.*[1] using laser anemometry in open channel flows, followed by the experiments using microbubble tracers by Rashidi and Banerjee.[2–4] Banerjee[5] reviews the state of the art in the field until 1990. The first direct simulation was reported by Lam and Banerjee.[6] The free surface was considered to be a rigid slip wall, i.e., as if the horizontal liquid layer resisted surface deformation due to very high gravitational and surface tension forces. Lam and Banerjee,[7] Komori *et al.*[8] and Handler *et al.*[9] presented direct simulations, though, Komori *et al.*[8] did the only work that, in principle, treats the full free surface boundary conditions. The work of Komori *et al.*[8] was still confined to surface deformations of small amplitude, so no significant differences compared to previous direct simulations were observed.

Open channel flows were taken as the basis for these calculations and experiments, primarily because a statistically steady state could be obtained. Banerjee[10] reviews this work up to early 1994, and indicates that the main structures consist of upwellings associated with bursts rising from the bottom boundary, downdrafts where the flow from adjacent upwellings meet, and "whirlpool-like" attached vortices (or more correctly "spiral eddies," since we will see later there is a weak downflow in the cores).

While the general features of these structures are clear, the details still have to be investigated; for example, the origin of the vortices, their evolution, and interactions.

When significant wind shear is imposed on the liquid surface, the surface is no longer "free" and entirely different structures result. Rashidi and Banerjee[3,4] have shown these structures are very like those in the boundary layer, i.e., low-speed streaky regions with bursts and sweeps occur just as in wall turbulence. These structures scale with the shear rate and kinematic viscosity, as at a solid wall, though Komori *et al.*[11] recently indicated that there appears to be a breakdown of scaling with the shear rate when three-dimensional waves appear.

Clearly when the externally-imposed (e.g., due to wind) stress is high enough, turbulence near a surface is predominantly three dimensional. However, for situations where the shear rate is small, i.e., the surface is free, Sarpkaya and Suthon[12] have conjectured that the turbulence structure might tend towards two-dimensionality. If true, this conjecture has interesting implication for computations of free-surface turbulence. For example, computations of the behavior of wakes far from vessels might be accomplished very economically if done two-dimensionally. In the region close to vessels or in other situations where turbulence is being generated, the structure will certainly be strongly three dimensional, even near a free surface. Therefore, the hypothesis regarding two-dimensionality is confined to a free-surface turbulence situation far from the region of turbulence generation.

The main objective of the present paper is to investigate the origin and evolution of free-surface turbulence structures. In particular, the formation of the attached vortices is of interest as nothing like this is seen at solid boundaries. The

a)E-mail: banerjee@anemone.ucsb.edu

 1070-6631/95/7(7)/1649/16/$6.00 © 1995 American Institute of Physics

Copyright ©2001. All Rights Reserved.

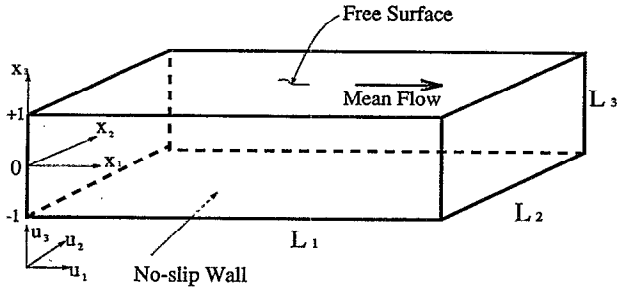

FIG. 1. Coordinate system of open channel flow.

conjecture regarding quasi-two-dimensionality of the flow near the surface is also examined. To this end, we start with a direct simulation of fully developed statistically-steady open channel flow bounded by a no-slip wall and a free surface that is treated as a rigid free-slip wall. While the latter assumption is certainly restrictive in the sense that deformations of the free surface may play a role in determining the nature of the flow, nonetheless, such simulations have proved in the past to capture many of the phenomena seen in experiments with waveless interfaces (see, for example, Lam and Banerjee[7]). In this regard, it should be noted that ship wakes often have a waveless "smooth" character (see Swean and Beris[13]), and many of the large-scale features may be captured in the approximation used here.

Once the fully-developed case has been established, the turbulence generation mechanism at the bottom is turned off by changing the boundary condition to free slip. This results in a decaying turbulence structure within the liquid stream, which is then investigated by direct numerical simulation. The main purpose here is to identify how the structures evolve at the free surface, in contrast to those in the central region of the channel flow, far from the region of generation.

II. NUMERICAL SIMULATION

A. Numerical implementation

Consider incompressible pressure-gradient driven flow between a no-slip wall and a rigid free-slip surface, as sketched in Fig. 1. The streamwise direction is denoted by x_1, the spanwise direction by x_2, and the wall-normal direction by x_3. The lengths of the computational box are given by L_1, L_2, and L_3, and the velocity components by u_1, u_2, and u_3. All quantities are nondimensionalized with the channel half-depth h and the effective shear velocity, u_e, defined as

$$u_e = \sqrt{\frac{h}{\rho}\left|\frac{dP}{dx_1}\right|}, \tag{1}$$

where $|dP/dx_1|$ is the magnitude of the mean pressure gradient which drives the flow. The effective Reynolds number is defined as

$$\mathrm{Re} = \frac{u_e h}{\nu}, \tag{2}$$

where ν is the kinematic viscosity. Periodic boundary conditions are applied in the x_1 and x_2 directions. As mentioned previously, a close physical analog of this problem is the flow of a waveless liquid stream in an open channel, such as in the studies by Rashidi and Banerjee.[2]

A pseudospectral method is employed to solve the problem. The periodic directions are treated with Fourier expansions and the wall-normal direction with a Chebyshev expansion. The time-dependent Navier–Stokes equations for flow are integrated numerically starting from an initial condition that may be a laminar flow with low-amplitude perturbations in some of the Fourier components. The simulation is carried on until statistically-steady turbulence results. It is known that the Reynolds stress distributions, skewness, flatness, and various other parameters for the numerical calculations correspond very well with experiments (Lam and Banerjee[6]). Such results have also been obtained by Kim *et al.*[14] and a number of other investigators.

Numerical procedures will not be discussed here as they are reported in Lam[15] and Lam and Banerjee.[2,7] The solution method is similar to that used by Kim *et al.*[14] in their simulation of turbulent channel flow, though the details are different as the computational procedures were developed independently. The method eliminates the pressure term from the Navier–Stokes equation by taking two curls, which results in a fourth-order equation for the velocity field. This is then solved for the wall-normal component of velocity together with the vorticity equations, which is also solved for the wall-normal component of vorticity. From these, then, using the definition of vorticity and continuity, the wall parallel velocity components can be calculated.

All calculations are done in wave-number space except for the multiplications, involving the nonlinear terms, which are done in physical space to avoid time-consuming convolutions. The procedure alternates between physical and wave-number space efficiently, by using the fast Fourier transform algorithm. Previous papers indicate that the efficiency of this method is far greater than performing the convolutions. Sufficient numbers of Fourier and Chebyshev modes, with appropriate dealiasing procedures, provide enough accuracy.

The shear Reynolds number, Re_τ, based on the depth of the liquid stream, the friction velocity at the no-slip wall and the kinematic viscosity is 171. For the calculations considered here, 64 Fourier modes are used in the streamwise direction, 64 in the spanwise direction, and 65 Chebyshev modes in the wall-normal direction. The computational box lengths are $L_1=4\pi$, $L_2=2\pi$, and $L_3=2$, scaled by the channel half-depth. While this resolution may appear modest in these days of 512^3 computations, they are quite sufficient for the problem at hand. This has been found (see Lam and Banerjee[7]) to give sufficient resolution to capture all essential features of the turbulent flow at this Reynolds number, which is about 6700 based on hydraulic diameter and mean streamwise velocity. Increased resolution ($\sim 128^3$) computations have also been done for the statistically-steady case without changing the results. In Fig. 2, we provide a comparison of typical results from a $64\times64\times65$ simulation with that of a $128\times128\times129$ simulation. The curves of one-

Copyright ©2001. All Rights Reserved.

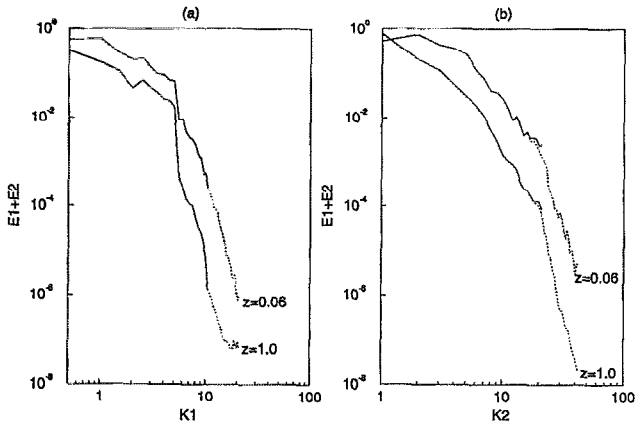

FIG. 2. One-dimensional energy spectra of the horizontal velocity component for 64×64×65 simulation (—) and 128×128×129 simulation (·····) at a time during the statistically-steady turbulence: (a) streamwise; (b) spanwise. The curves are plotted for two horizontal planes located at different distances from the free surface. The wave numbers are $K_1=i2\pi/L_1$ and $K_2=j2\pi/L_2$ for streamwise and spanwise directions, respectively. The spectra are identical at the low wave numbers.

dimensional energy spectra of horizontal velocity, for two simulations, are indistinguishable except at the highest wave numbers. A detailed summary of the parameters for all simulations is given in Table I.

The results of the direct numerical simulations may be viewed in many different ways. One of these is to visualize the instantaneous streamlines on planes in various orientation and locations, e.g., at the free surface and cross stream to the flow. Another method is to use a scalar measure to identify vortices as discussed below.

B. Vortex identification

A vortex is an entity that is conceptually easy to appreciate, but difficult to identify using numerical algorithms. However, vortices are often the persistent structures in a turbulent flow and mechanistic modeling must be based on an understanding of their origin and subsequent behavior. Therefore, a relatively unambiguous method of identification is needed. Note that instantaneous streamlines produced by integrating the velocity vector field resolved onto some chosen plane may exhibit either closed orbits or, perhaps, spirals through which it might be thought that vortices pass. Also a vortex may exist in regions where isovorticity curves bunch up. These qualities are usually thought to be the signatures of a vortex. In the present study, we have to identify and trace vortex motions not only in a three-dimensional space, but also in time. Clearly, the most convincing way to see a vortex is to plot the instantaneous streamlines. Since the vortex structures in the turbulent flow are three dimensional, the two-dimensional streamlines on a particular plane can only indicate the vortices whose axes are nearly perpendicular to that plane. In the region close to the free surface, in which we are mostly interested, the dominant orientation of the attached vortices would be normal to the free surface and so this type of visualization is useful. The two-dimensional streamlines in the x_1-x_2 planes at different distance from the free surface would then show the downward extension of such "attached" vortices.

However, to study the spatial structure of such vortices, in general, it is useful to have a scalar measure, whose value gives the strength and the direction of the vortex and whose distribution gives the location and shape of the vortex. Such a measure, combined with streamlines, could then be used to identify and follow the vortices as they evolve in space and time, using computer visualization. Unfortunately no perfect scalar measure of a vortex is known. Vorticity itself is a problematic identifier, since it cannot distinguish between shear layers and vortices. (Any shear layer has vorticity, whether or not vortices are present.) In the problem under consideration, the flow patterns are so complicated that vorticity contours by themselves cannot provide clear information. Bundles of vortex lines are better identifiers but it is difficult to develop a measure for what constitutes a "bundle."

An alternative measure of vortices has been developed by considering expansions around critical points in the flow field (see Perry and Chong[16]). The local topology of the flow can be found by examining the eigenvalues of the velocity gradient tensor or the rate-of-deformation tensor $\partial u_i/\partial x_j$. When this tensor has complex eigenvalues, a vector, $\mathbf{\Omega}$, related to streamline rotation, may be established on the basis of the eigenvectors for each eigenvalue (see Hirschberg[17] for a detailed discussion of the method). This vector, locally, represents the strength and direction of the rotation of the streamlines. This method is based on "critical point" theory. Chong *et al.*[18] gave a general description of this theory in classifying three-dimensional velocity fields. Hunt *et al.*[19] suggested the second invariant of the velocity gradient tensor, defined as

$$\Pi = s_{ij}s_{ij} - \tfrac{1}{2}\omega_i\omega_i \tag{3}$$

is a scalar measure to locate vortices in space; s_{ij} and ω_i are the rate-of-strain tensor and vorticity, respectively. Therefore, large negative values of Π indicate regions in the flow where vorticity dominates over strain. McWilliams[20] used this method to decompose the two-dimensional turbulent flow into two components, cascading turbulence and isolated, hard-core vortices. Actually, using $\mathbf{\Omega}$ and Π as vortex indicators are nearly identical due to the fact that wherever the value of Π is negative, $\partial u_i/\partial x_j$ has complex eigenvalues.

TABLE I. Flow condition and computational parameters.

Case	Re	Re_τ	$L_1^+\times L_2^+\times L_3^+$	Mesh	Δt	N_{step}
Steady	60.4	171	1074×537×171	64×64×65	1×10^{-3}	6500
Decaying	60.4	171	1074×537×171	64×64×65	1×10^{-3}	11000
Testing	60.4	171	1074×537×171	128×128×129	4×10^{-4}	8000

Copyright ©2001. All Rights Reserved.

The postulate behind this method is that a vortex core is a region where the vorticity is sufficiently strong to cause the rate-of-strain tensor to be dominated by the rotation tensor, i.e., the rate-of-deformation tensor has complex eigenvalues.

Another measure of vortices is pressure. Generally, pressure has relatively low values in the center of a region of strong rotational fluid motion. The fluctuating pressure field in an incompressible turbulent flow can be calculated by solving a Possion equation, once the velocity field $\mathbf{u}$ is known. The size of the pressure depression gives a measure of the strength of a vortex. Although this seems rather obvious, the pressure is rarely used to locate vortices in experiments, since it is difficult to measure. Furthermore it is not guaranteed that every pressure minimum is associated with a vortex. One really needs a confirming plot of the local velocity vector or the streamlines in a plane perpendicular to the axis of the vortex, and in a reference frame moving with the vortex, to be certain that a vortex does exist. Sandham and Kleiser[21] used the pressure as an indicator for vortices. They studied the transitional stage to turbulence in channel flow, in which vortices are growing from a laminar flow. Since the flow is dominated by a few strong vortices, the "background" is relatively clean. Therefore, the pressure turned out to be a good indicator in their study. However, this is not always the case.

In fact, the pressure, p, and the second invariant of the velocity gradient tensor, Π, are related by the following equation:

$$\nabla^2 p = -\Pi. \tag{4}$$

As pointed by Brachet,[22] the vorticity concentration, which is the negative part of Π, acts like a source of low pressure, while the energy dissipation concentration, which is the positive part of Π, acts as a source of high pressure. Therefore, in the regions where Π is highly negative, the pressure will be relatively low. This concept had been used numerically by Brachet[22] and experimentally by Douady *et al.*[23] to study the spatial correlation between turbulent activity and low-pressure regions.

In the present study, we have found that, in the case of fully developed turbulent channel flow, both the streamline rotation, $\mathbf{\Omega}$, and the fluctuation pressure p' are unable to give a clear picture of the spatial structure of the vortices close to the free surface. It is also found that the pressure is a good indicator only for strong vortices. In the wall region, where turbulence is strong and the vortices are mostly quasistreamwise, $\mathbf{\Omega}$ and p' are both good indicators. In the region close to the free surface, where the turbulence is relatively weak, the pressure is unable to distinguish the relative weak vortices from the regions where low pressure exists due to other reasons. However, in decaying turbulence, which will be discussed in Sec. IV, spatially sparse concentrations of vorticity (coherent vortices) become the dominant feature of the flow pattern in the region close to the free surface. Vorticity, streamline rotation and pressure are all good scalar measures in this case. The conclusion is that the different measures of a vortex are useful in different regions and stages of the flow—i.e., we have not been able to find an universal measure. Nevertheless, a carefully chosen scalar indicator, spot checked at various locations by calculating the instantaneous streamlines, is able to give reliable information regarding vortices in most flows.

III. STRUCTURES IN STATISTICALLY-STEADY-STATE TURBULENCE

In this section we will focus on turbulence structures in the region close to the free surface of statistically-steady open channel flow, e.g., in a situation where the root-mean-square (RMS) of the fluctuating velocities $\overline{u_i'^2}$, the Reynolds stress $\overline{u_1' u_3'}$ and higher-order statistical measures do not change with time. As the channel depth is 171 wall units, the free surface region may be thought of (in a heuristic sense) as a layer about 20 to 30 wall units thick below the surface. It is this region which we will examine, in more detail, later.

Figures 3(a)–3(c) show typical turbulence structures in the channel. Figure 3(a) is the instantaneous streamlines on a cross-sectional plane in fully developed channel flow. The free surface is at the top and the no-slip boundary is at the bottom. The view is of a cross-sectional plane in the spanwise direction, i.e., a x_2-x_3 plane, where x_3 is the wall-normal direction. The mean streamwise flow goes into the paper. The colors represent the values of $\mathbf{\Omega}_1$, which is the streamwise component of streamline rotation $\mathbf{\Omega}$. The color blue (negative values) indicates anticlockwise rotation of vortices. The color red–yellow (positive values) indicates the clockwise rotation of vortices. Note that the vortices indicated are normal to the plane, i.e., quasistreamwise structures, particularly in regions close to the wall. Such structures have been observed by many other investigators and discussed, in particular, by Robinson.[24] At the region close to the free surface, one can also observe upward and downward flows. That the wall structures are essentially quasistreamwise is further evident from Fig. 3(b) where the isosurfaces of the magnitude of streamline rotation, $|\mathbf{\Omega}|$, are shown. The isosurfaces are colored again by the value of $\mathbf{\Omega}_1$. These vortices are about 100 wall units in length. Though it is not shown here, the topology of the streamlines on x_2-x_3 planes cutting through the quasistreamwise vortices indicated by the isosurfaces of $|\mathbf{\Omega}|$, show that this measure works well in this case.

Figure 3(c) shows the flow pattern seen by moving with the flow and looking down at the free surface. The instantaneous streamlines together with the color contour map of the fluctuating surface-normal velocity, u_3', show three distinct regions. The first are the attached vortices. The second are stagnation lines where streamlines from two different sides converge. The third are a regions of divergence of streamlines, which we call upwellings. The colors in the figure indicate the instantaneous velocity component normal to the free surface, with blue representing negative values (which are downwards from the surface) and green or red representing positive values (which are upwards to the surface). Since the normal velocity, u_3', is zero at the free surface itself, the colors refer to values on a horizontal plane one wall unit below. In this figure, the blue, which is the predominant color along the stagnation lines, indicates a down flow or a downdraft, whereas yellow or red, which overlap the regions

Copyright ©2001. All Rights Reserved.

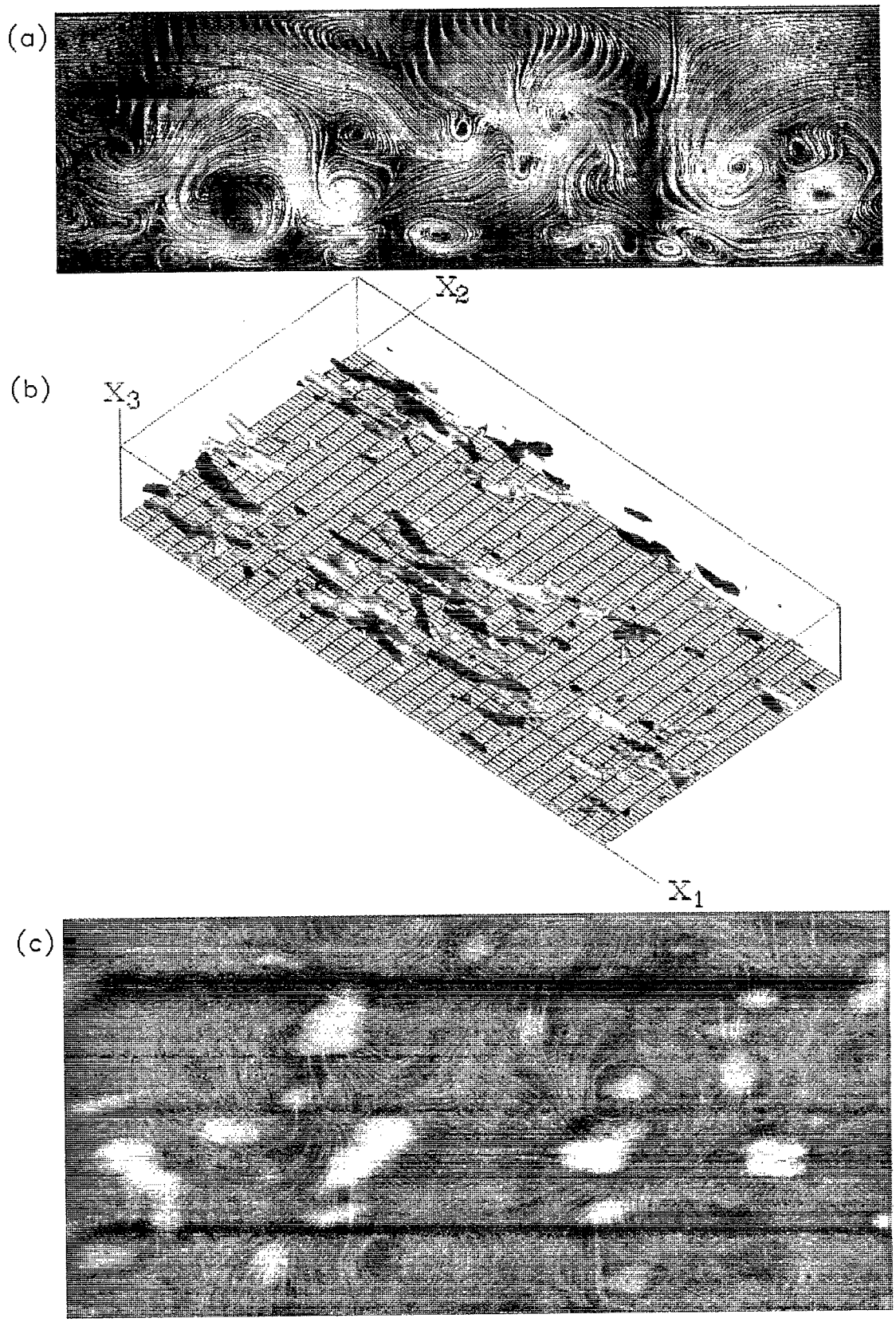

FIG. 3. Turbulence structures in channel flow. (a) End view: streamlines and color contours of Ω_1. (b) three-dimensional view: isosurfaces of $|\Omega|$ colored by Ω_1. (c) Top view on free surface: streamlines and color contours of surface-normal velocity, u_3'.

Copyright ©2001. All Rights Reserved.

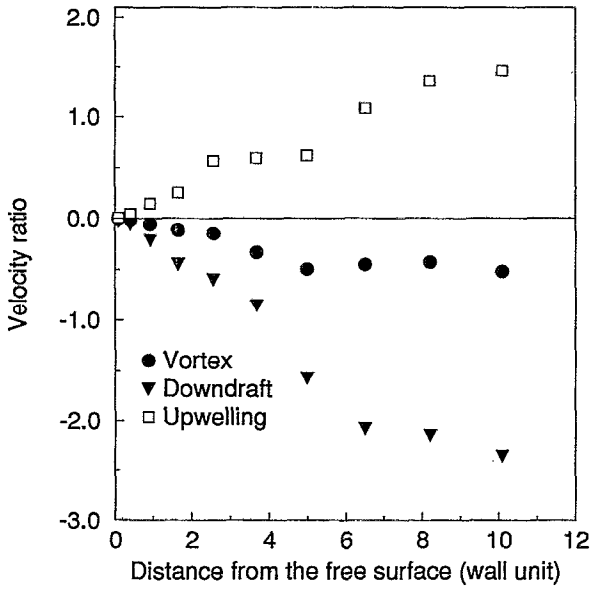

FIG. 4. The ratio of the averaged magnitude of the surface-normal velocity to that of the surface-parallel velocity in the regions of vortex, upwellings, and downdraft at several planes near the free surface. The values are measured by using the velocity field for plotting Fig. 3(c).

with divergent streamlines, indicates upward motion. Though we do not show it here, it is evident from cross-section plots, as shown in Fig. 3(a), that the streamlines in the downdraft regions, under the stagnation lines, also indicate strong downward motion. In rough terms, therefore, the pattern at the free surface can be divided into upwellings which are yellow–green, downdrafts which are blue, and vortices which occur quite often at the edges of the upwellings. This is the essential taxonomy which is supported by experiments to be reported in a subsequent paper by Gupta *et al.*[25] A quantitative measure of the surface-normal motion in the regions of vortex, upwelling, and downdraft is provided by Fig. 4, where the ratios of the averaged surface-normal component of velocity to that of the surface-parallel component are shown for each of the regions, at several planes near the free surface. The velocity field used for this figure is the same for Fig. 3(c). The values are calculated by averaging the values of velocities, separately within vortices, upwellings and downdrafts. Strong downward and upward motions, with vertical to horizontal velocity ratios substantially greater than one, are observed in downdrafts and upwellings, respectively. As expected from the free-surface boundary condition, the magnitude of these motions decreases as the flow approaches the free surface. It can also be seen that most of the vortices are associated with weak downward motion. The small value of the velocity ratio in the vortices indicates their quasi-two-dimensional character. However, because of the the weak downflow the vortical regions should perhaps be identified as spiral eddies rather than attached vortices.

The structure and generation of these attached vortices, as well as their interaction with the free surface, are further studied by looking at the images of flow visualization shown in Fig. 5. The spatial structure of these vortices can be seen in Fig. 5.1 where the isosurfaces of the second invariant of the velocity gradient tensor, Π, is used as a vortex indicator. The isosurfaces are colored by the value of surface-normal component, Ω_3, of the streamline rotation vector $\mathbf{\Omega}$ to give the direction of rotation. The color yellow–green and blue indicate anticlockwise and clockwise rotation of the attached vortices, respectively. The flow pattern on the free surface is also shown by the streamline plot. The isosurfaces are plotted in a layer about 13% of the channel depth down from the free surface, corresponding to a depth of 22 wall units. It is evident from the figure that these vortices are primarily in a direction that is surface normal, i.e., the vortices hang downwards. Therefore, we call them "attached" vortices. It is also clear from this figure that there no quasistreamwise vortices near the surface indicated by Π contours (we may recall that these were the dominant vortical structures near the wall). There is, therefore, a considerable contrast in the orientation of the vortices between that of the wall and that of the free surface. In some sense, what is seen follows from the fact that ω_1 and ω_2 must vanish at the free-slip surface, as must $\partial\omega_3/\partial x_3$. Therefore, ω_1 and ω_2 are proportional at best to distance from the free surface, and ω_3 is relatively constant.

The three structures, viz. vortices, upwellings, and downdrafts, are closely related phenomena. As shown in Figs. 3(c) and 5.1, the vortices mostly occur at the edges of the upwellings. The qualitative mechanisms behind generation and extinction of an attached vortex are now explored. We will first focus on a portion of the flow field on the free surface and trace the formation and annihilation of an attached vortex. Figure 5.2 shows the streamlines on a portion of free surface and the continuous color contours of the fluctuating normal velocity u_3 on a x_1-x_2 plane at $x_3^+=1$ from the free surface. The central region of Fig. 5.2(a) shows the initial stage of an upwelling rising up towards the free surface, as a result of a burst from the wall region. The red spot at the center of the figure indicates an upwelling. At this moment, it has not reached the free surface. Due to the upward motion, the streamlines on the top of the upwelling, which were previously parallel, start to be pushed outward. They radiate outward as in Figs. 5.2(b) and 5.2(c), showing that the upwelling has reached, or is very near, the free surface. One can also see that a bundle of convergent streamlines forms at the edge of upwelling. This streamline-convergence region is colored blue indicating down flow. The edge of an upwelling is usually a high shear region, particularly in the region between two upwelling which are closely adjacent. Since instabilities may occur in such high shear regions, a vortex is most likely to be initiated there, i.e., at the edges of upwellings. The generation of a vortex can be clearly seen from Figs. 5.2(a) to 5.2(d). (In the region between two upwellings, one at the center and another at the right-low corner of the image, a vortex is seen to grow). At the time of Fig. 5.2(d), this vortex is well formed. From Figs. 5.2(d) to 5.2(h), one can see another vortex generated at the left edge of the central upwelling. During the same period of time, the first vortex (formed earlier), is being annihilated by another upwelling. This mode of annihilation is common, and is also seen experimentally by Gupta *et al.*[25]

Copyright ©2001. All Rights Reserved.

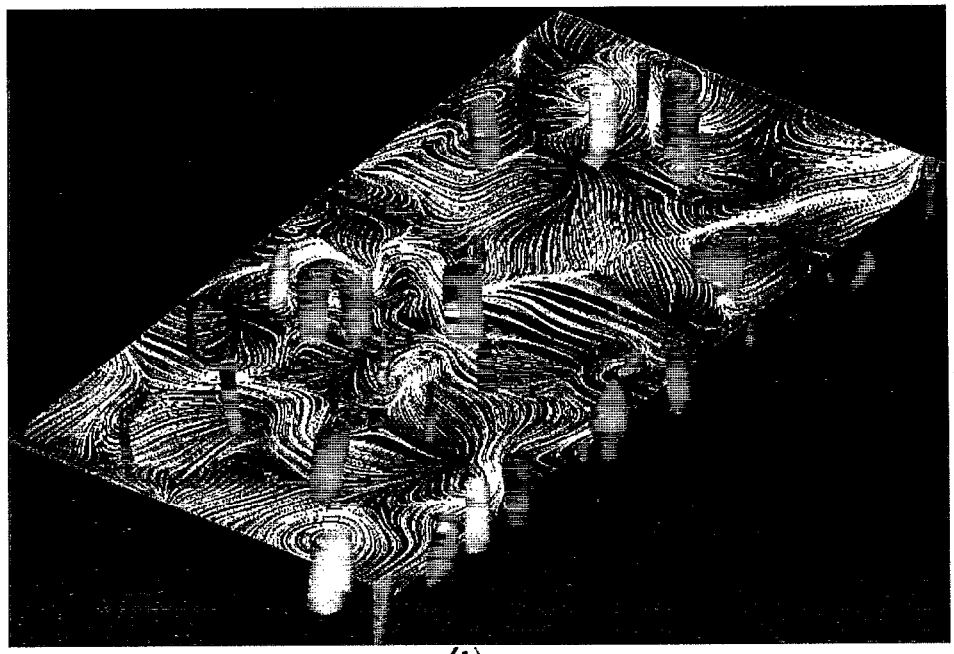

(1)

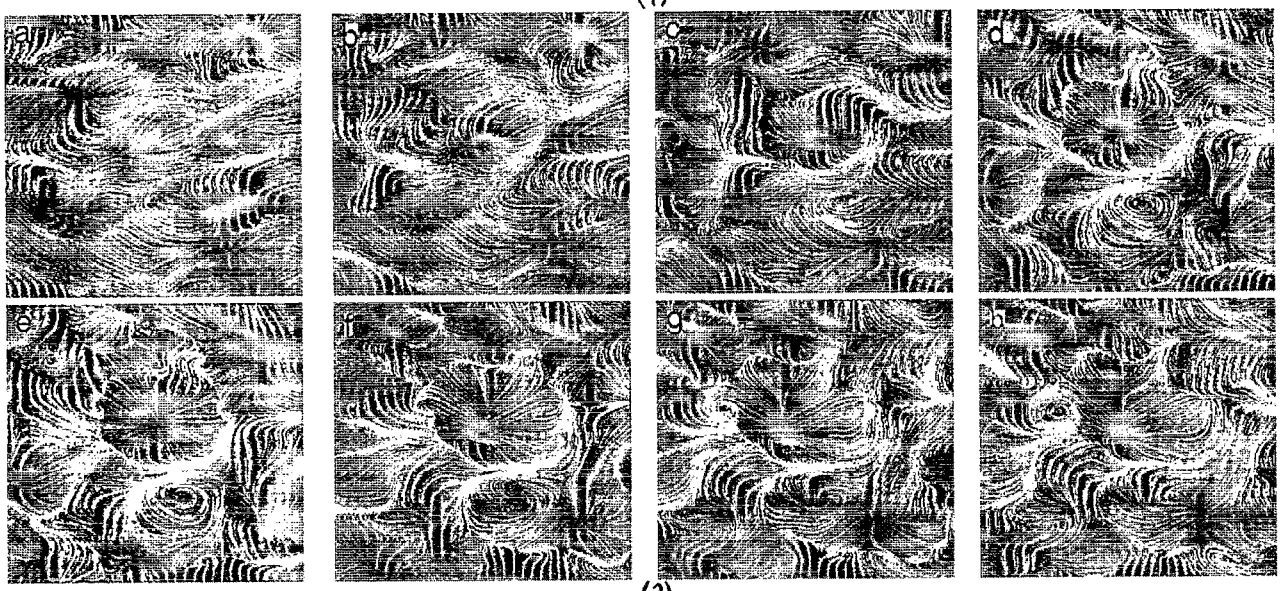

(2)

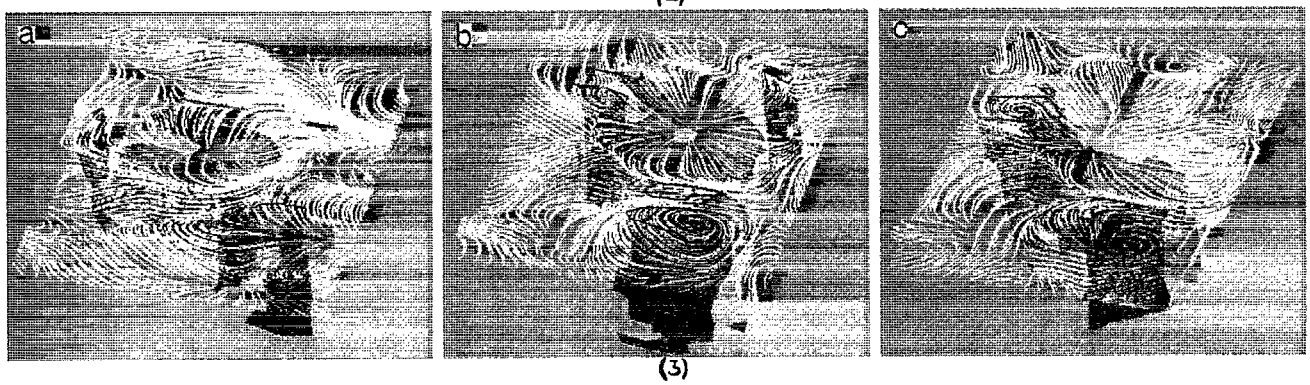

(3)

FIG. 5. Structure and generation of attached vortices. (1) Spatial structure of the vortices attached to the free surface. (2) Formation of an attached vortex due to an upwelling impinging upon the free surface. Time increases from (a) to (h). (3) Vortex generation and annihilation due to the reorientation of surface-parallel component of vorticity to surface-normal component of vorticity as the free surface is approached.

Copyright ©2001. All Rights Reserved.

Figure 5.3 illustrates, by considering the three-dimensional field under the free surface, the major stages of the evolution of an upwelling, and the generation and extinction of attached vortices at edges of upwellings. The isosurface of surface-parallel components of vorticity, $\sqrt{\omega_1^2+\omega_2^2} = 2.5\bar{\omega}_0$ ($\bar{\omega}_0$ is the averaged value of the magnitude of surface parallel components of vorticity in the region), the positive surface-normal vorticity, $\omega_3=2\bar{\omega}_3$, and the negative surface normal vorticity, $\omega_3=-1.5\bar{\omega}_3$, are denoted by green, red, and blue colors, respectively. These images are snapshots of a statistically-steady-state turbulent flow over a sequence of time steps. (For a fully developed statistically-steady-state turbulent flow, the origin of time is irrelevant.) The yellow lines are instantaneous streamlines on the free surface. The view is from below the free surface, and the mean flow is moving from the left of the page to the right. These flow visualizations have been focused on the central upwelling in Fig. 5.2 to clarify what is happening below the free surface. The extent of the plots in the streamwise, spanwise, and surface-normal direction are 200, 220, and 30 in wall units, respectively.

Figure 5.3(a) shows the initial stage of an upwelling, which causes high horizontal vorticity near the surface because of jet-like impingement. As the upwelling reaches the free surface, a donut-shaped region of high vorticity is formed, as shown in Fig. 5.3(b). This is not a vortex ring, as is evident from an examination of streamlines on surface-normal planes (not shown here). When this donut-shaped region interacts with the free surface, it induces a surface-normal component of vorticity that connects with the free surface forming nascent vortices at the edge of the upwelling as shown by the red and blue tubes. It is seen that the two attached vortices have opposite directions of rotation. (The blue–black color denotes clockwise rotation while the red denotes anticlockwise rotation.) The annihilation of the blue vortex by a second upwelling can also be observed in Fig. 5.3(c). At the lower right-hand edge of the figure, the outward radiating streamlines indicate impingement of another upwelling (not shown). It is clear that the flow induced by the second upwelling is strong enough to overwhelm the motion of the blue–black vortex. The connection process is similar to the cases studied by Dommermuth[26] where a pair of vortex tubes interact with a free surface and the normal connections of vorticity with the free surface give rise to whirls (see also Rood[27]).

IV. STRUCTURES IN DECAYING FREE-SURFACE TURBULENCE

In the previous sections, the mechanisms leading to formation and annihilation of attached vortices for the cases of statistically steady-state turbulence, were discussed. However, an issue of some interest is what happens to free-surface turbulence far from the region of turbulence generation, e.g., in the wake of a vessel. Is it quasi-two dimensional?

In order to investigate such behavior, we simulated a case where the no-slip boundary condition on the bottom solid wall is changed to a free-slip boundary condition after

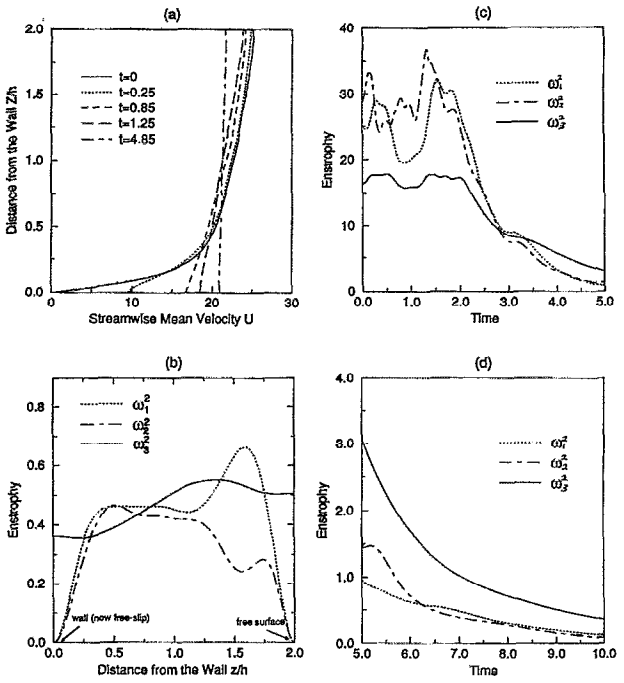

FIG. 6. Time evolution of flow quantities during the decaying process. (a) Mean streamwise velocity; (b) distribution of enstrophy along the depth of channel at 5 nondimensional time units after the beginning of decay; (c) and (d): enstrophy average in a thin layer next to the free surface with a thickness of about 10% of the channel depth.

the flow reaches a statistically steady state. At the same time the pressure gradient which drives the flow is turned off. Physically, this changing of boundary conditions is equivalent to eliminating the mechanism of turbulence generation. The flow in the channel begins to decay.

In the following paragraphs, the moment when the no-slip boundary condition is changed will be denoted by $t=0$. The time is still scaled by the effective shear velocity, u_e, at and the half-depth of the channel h. Of course as the decay proceeds these scaling parameters lose their physical significance. Nevertheless they provide a measure which may be related to the original statistically steady flow.

Once the bottom boundary condition is changed to free slip, the velocity profile decays, as indicated in Fig. 6(a). Within about 5 nondimensional time units, the velocity profile is nearly flat. [The distribution of the enstrophy within the liquid stream is shown in Fig. 6(b) after 5 time units into the decay.] It is clear that in the central region of the liquid stream, the enstrophy components in the streamwise, spanwise, and surface-normal directions are about equal. However, close to the free surface and close to what was originally the no-slip wall, one can see that the surface-parallel components of enstrophy rapidly decay whereas the surface-normal component is substantial. The time evolution of the enstrophy averaged in a thin layer close to the free surface (about 10% of the channel depth) is shown in Figs. 6(c) and 6(d). It is clear that the enstrophy components in the surface-parallel directions decay very rapidly and the only component left is in the surface-normal direction. Recall that

Copyright ©2001. All Rights Reserved.

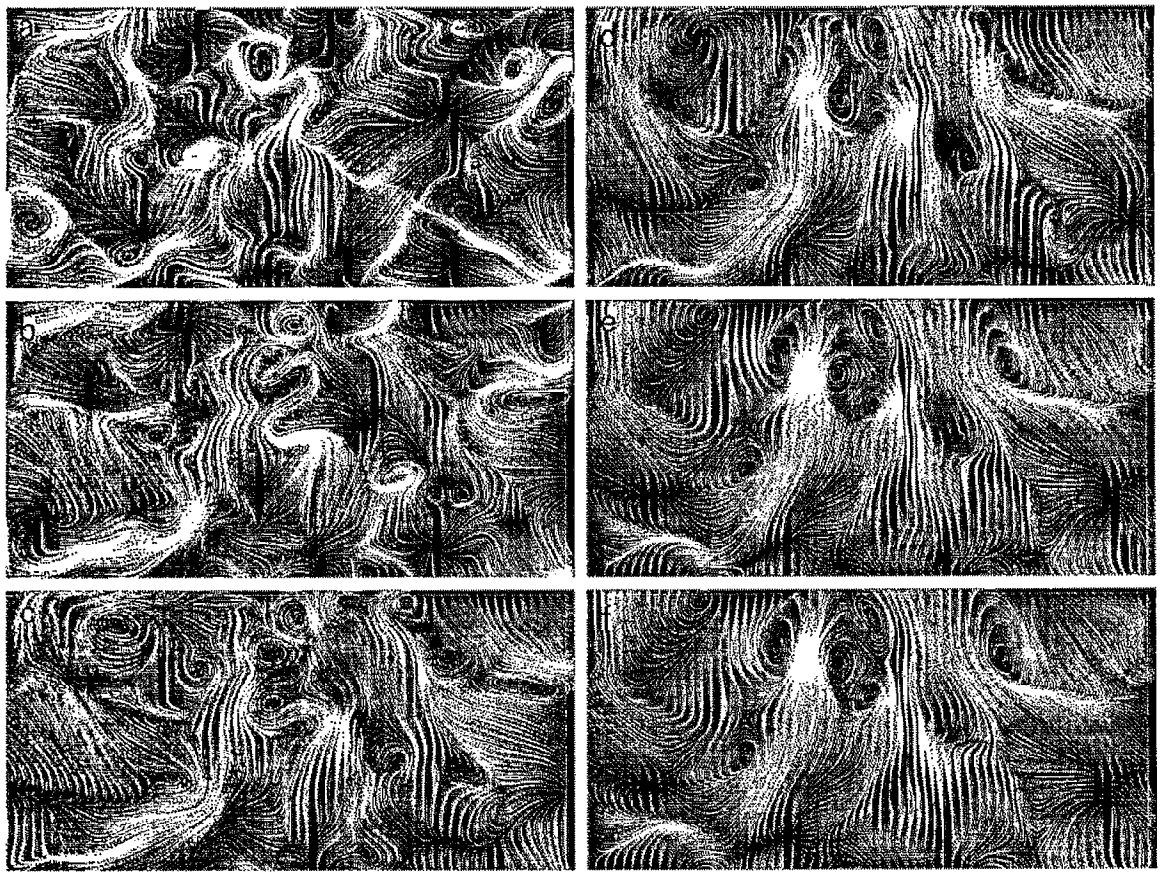

FIG. 7. Time evolution of flow pattern on the free surface during the decaying process: (a) $t=3.69$; (b) $t=4.58$; (c) $t=6.10$; (d) $t=7.17$; (e) $t=8.33$; (f) $t=8.91$. In one unit of nondimensional time, the mean flow goes through a distance of twice the length of channel, $L_1=4\pi h$.

by a nondimensional time of about 5, the velocity profile in the liquid stream has become essentially uniform so there is no turbulence generation. At this time, the streamwise and spanwise vorticity is virtually zero near the surface whereas the surface-normal vorticity is substantial and decays only slowly with time after that.

The flow pattern observed on the free surface undergoes an evolution as shown in Fig. 7. This is a sequence of streamlines at the time instance given in the figure caption, where $t=0$ denotes the time when the no-slip boundary condition at the wall is removed. In the first plot, Fig. 7(a), one can clearly discern the very intense stagnation lines which are downdrafts and regions of upwelling where the streamlines fan outwards to the stagnation lines. One can also discern the vortices in the regions near the stagnation lines, i.e., at the edges of the upwellings. As the shear at the bottom boundary decreases, turbulence generation is suppressed and the upwellings and downdrafts become less pronounced. By the time in Fig. 7(d), one does not perceive very strong stagnation lines or upwellings but the vortices continue to evolve. In particular, the vortices pair and coalesce, forming fewer and larger vortices. By noticing the time spans between the plots, one can see that these vortices are long-lived.

Figure 8 shows, in more detail, the pairing and merging of the vortices. In this figure, the streamlines are plotted on a portion of free surface with the colors representing the strength of the normal component of vorticity. The blue color denotes negative values of surface-normal vorticity, which corresponds to clockwise motions. The red and yellow spots indicate positive values of normal vorticity, which corresponds to anticlockwise motions. This figure gives a sequence of flow visualizations during the decay process, from which one can clearly see that vortices rotating in the same direction tend to merge whereas those in opposite directions pair. A merger of several vortices can be observed in the lower right-hand corner (the blue vortices). For vortices of opposite sign a stable configuration is established as for the two red–yellow and one blue shown in the lower and midleft region of the figure. It can be observed from Figs. 7 and 8 that these vortices are very stable. These long-lived isolated concentrations of vorticity observed here are consistent with those of the two-dimensional turbulent flows studied by McWilliams,[20,28] Brachet *et al.*,[29] and Santangelo *et al.*[30]

The previous discussion has been primarily qualitative and it is worth discussing quantitative aspects such as the energy spectra, energy transfer between wave numbers and evolutions of length scales. From the previous studies of two-dimensional turbulence, upcascading of energy is confined primarily to large scales. This reverse cascade of energy can be investigated by looking at the length scales in the flow. The integral scale

Copyright ©2001. All Rights Reserved.

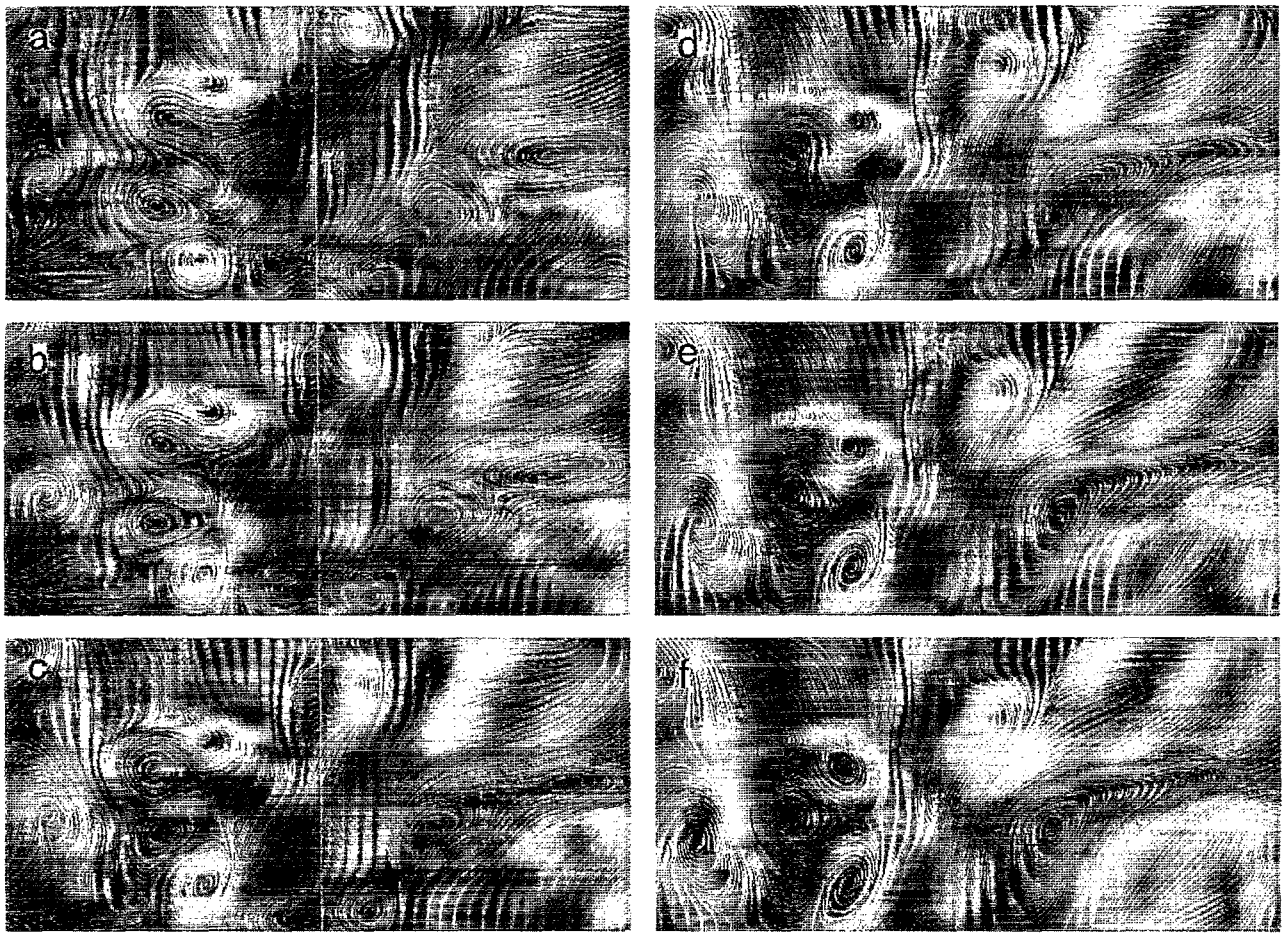

FIG. 8. Vortex evolution on the free surface: instantaneous streamlines and color contour of surface-normal component of vorticity, ω_3. The positive value (anticlockwise rotation of vortex) and negative value (clockwise rotation of vortex) are denoted by red–yellow and blue, respectively. Time increases from (a) to (f). The figure shows a portion of the whole surface.

$$l_{ij}=\frac{\int_0^\infty k_j^{-1}E_i(k_j)dk_j}{\int_0^\infty E_i(k_j)dk_j} \tag{5}$$

and the Taylor microscale

$$\lambda_{ij}=\sqrt{\frac{\int_0^\infty E_i(k_j)dk_j}{\int_0^\infty k_j^2E_i(k_j)dk_j}} \tag{6}$$

are shown in Fig. 9. The length scales for the surface-parallel motion at the free surface increase substantially during decay. From the length scales it is clear, of course, that the turbulence structure, even at the surface plane is anisotropic, i.e., the scales are different in the x_1 and x_2 directions.

Figures 10(a) and 10(b) show the evolution of the one-dimensional, both streamwise and spanwise, energy spectra for the surface-parallel velocity fluctuations at the free surface during the decay process. The energy spectra of the statistically steady case, i.e., fully developed channel flow before the decay starts, are shown here (indicated by curves corresponding to $t=0$) for comparison. Two inertial ranges $k^{-5/3}$ and $k^{-3.5}$, shown for the steady state, are consistent with the theoretical works by Kraichnan[31] and Batchelor,[32] and the experimental work by Narimousa *et al.*[33] By comparing Figs. 10(a) and 10(b), one can see that the behavior of turbulence in the streamwise and spanwise direction are very consistent. It also shows that, as the flow decays, the energy spectra changes rapidly primarily by steepening at large k

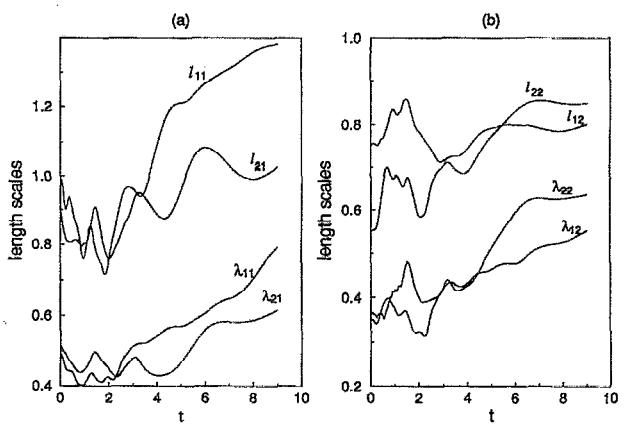

FIG. 9. Time evolution of length scales (integral scales and Taylor microscales) on the free surface during the decaying process: (a) streamwise scales; (b) spanwise scales.

Copyright ©2001. All Rights Reserved.

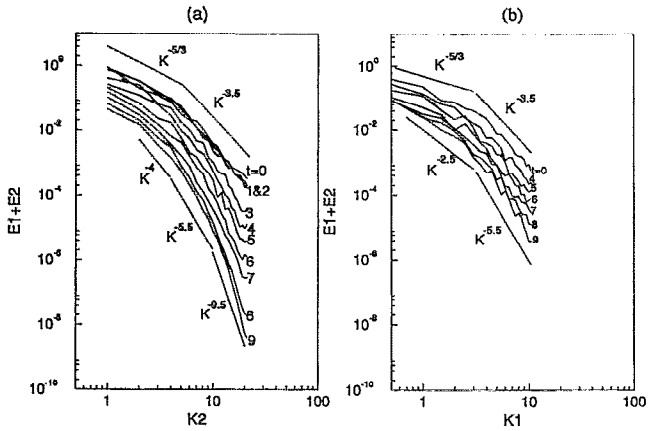

FIG. 10. Time evolution of one-dimensional energy spectra of the surface-parallel velocity components during the decaying process: (a) spanwise; (b) streamwise.

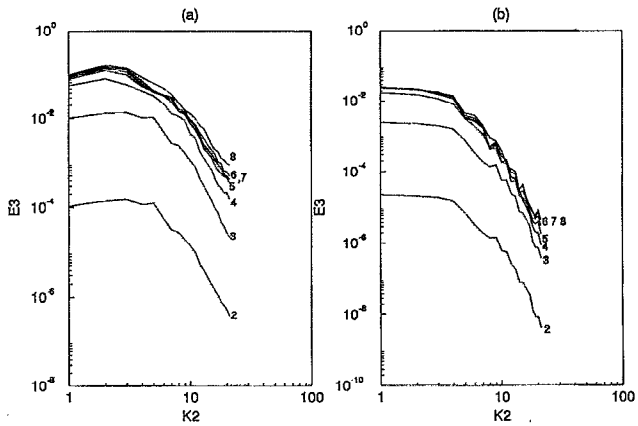

FIG. 12. One-dimensional energy spectra of surface-normal component of velocity at various distance from the free surface: 1 for $z=0.0$; 2 for $z=0.01$; 3 for $z=0.12$; 4 for $z=0.4$; 5 for $z=0.62$; 6 for $z=0.71$; 7 for $z=0.8$; 8 for $z=1.0$; (a) steady state; (b) decaying flow at $t=3.5$.

from the initial shape of $k^{-3.5}$ for the steady state. There is an increase in the slope of the decaying portion of the spectrum from $k^{-3.5}$ to about k^{-9}. The increase in slope for decaying two-dimensional turbulence follows this behavior rather closely. In essence, there is a sort of reverse cascade with energy in the high wave numbers decaying rapidly, but low wave numbers (large vortices) decaying much more slowly.

Direction-related aspects of the energy spectra are shown in Figs. 11 and 12. In order to see the evolution of turbulence, the energy spectra for surface-parallel and surface-normal velocity of the statistically steady-state turbulence are shown in Figs. 11(a) and 12(a), respectively, as baselines for comparison. The spectra for four different horizontal planes, ranging from the free surface to the center plane of the channel, are shown. First note that as we go down from the free surface the low wave-number spectra no longer exhibit a $k^{-5/3}$ range in Fig. 11(a). Also, the differences in spectra in Figs. 11(a) and 12(a) reflect the fact that the turbulence is anisotropic in the surface-normal direction. The blocking effect due to the image vortex field calculated by Hunt and Graham[34] is evident (see, also, Banerjee[6]). Similar behavior is also obtained by Handler *et al.*[9] In Fig. 11(b), the energy spectra for surface-parallel components of velocity in decaying turbulence at time corresponding to $t=3.5$ is shown. One can see that at this time into the decay, the energy spectra of the horizontal velocities at different planes have become essentially identical except at the lowest wave numbers. For the low wave numbers, the region near the channel center still does not exhibit a $k^{-5/3}$ behavior, but the high wave-number spectra at various depths become identical. Figure 12(b) shows that the spectra for the surface-normal velocity undergoes little change except for decay. At high wave numbers, for the planes close to the free surface, the spectra shift from $k^{-5/3}$ to $k^{-4.5}$, which is due to the fact that the flow is undergoing a decay process, as we have seen in Fig. 10(a). The spectra of streamwise velocity at various depths indicate that the $k^{-5/3}$ region propagates downwards during decay, i.e., the quasi-two-dimensional region thickens.

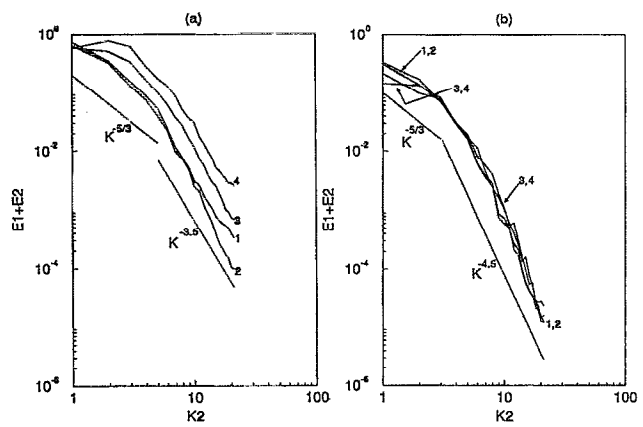

FIG. 11. One-dimensional energy spectra of surface-parallel components of velocity at various distance from the free surface: 1 for $z=0.0$; 2 for $z=0.12$; 3 for $z=0.62$; 4 for $z=1.0$; (a) steady state; (b) decaying flow at $t=3.5$.

In fact, the quasi-two-dimensional behavior of the flow near the free surface is related to the anisotropy in the corresponding regions. A symmetric tensor, **B**, defined as

$$b_{ij}=\frac{\overline{u_i' u_j'}}{u_k' u_k'}-\frac{\delta_{ij}}{3} \tag{7}$$

is used here as a measure of the anisotropy of a turbulent flow. Notice that the trace of **B** is zero. It can be shown[35] that, as two-dimensional turbulence is approached, we have

$$\epsilon=\tfrac{1}{9}+\Lambda_2+\Lambda_3\to 0, \tag{8}$$

where Λ_2 and Λ_3 are the independent invariants of **B**, defined as[36]

$$\Lambda_2=[\mathrm{tr}(\mathbf{B})]^2-\mathrm{tr}(\mathbf{B}^2),$$

$$\Lambda_3=[\mathrm{tr}(\mathbf{B})]^3-3\ \mathrm{tr}(\mathbf{B})\mathrm{tr}(\mathbf{B}^2)+2\ \mathrm{tr}(\mathbf{B}^3),$$

Copyright ©2001. All Rights Reserved.

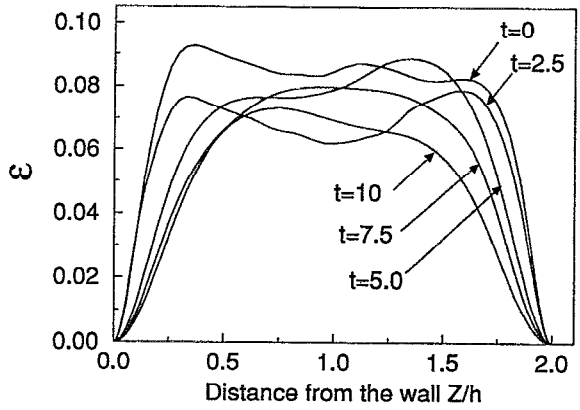

FIG. 13. Value of anisotropy criterion for turbulence, ϵ, as defined by Eq. (8), in channel at various time during the decay process. Turbulence starts to decay at time of $t=0$.

in which "tr" denotes the trace of the tensor in the argument. In Fig. 13, the distribution of ϵ with the channel depth during the decay process is shown. It can be seen that as the turbulence decays, ϵ monotonically approaches its two-dimensional limit at both the free surface and the free-slip wall (at the bottom). Although the turbulence in the center of the channel still remains quite a three-dimensional one, the quasi-two-dimensional region is clearly deepening into the three-dimensional core. This behavior is consistent with the spectra shown in Figs. 10 and 11.

The two-dimensional character of turbulence within the surface region can be further investigated by examining the kinetic energy transfer spectra. The transfer function $T(\mathbf{k},x_3)$ is defined as

$$T(\mathbf{k},x_3)=\Re[u_i^*(\mathbf{k},x_3)N_i(\mathbf{k},x_3)]. \tag{9}$$

The nonlinear term $N_i(\mathbf{k},x_3)$ consists of the advection and pressure terms; $u_i^*(\mathbf{k},x_3)$ is the complex conjugate of the velocity component in wave space with $\mathbf{k}=(k_1,k_2)$. Physically, $T(\mathbf{k},x_3)$ represents energy redistribution by nonlinear interactions. Figure 14 shows the spectra of $T(\mathbf{k},x_3)$ on different horizontal planes from the free surface. At the surface region, as shown in Fig. 14(a), the spectra is dominated by net reverse transfer of energy to the large scales which indicates two-dimensional character. As one goes down from the free surface, shown in Fig. 14(b), the dominating feature becomes a net forward transfer of energy from the large scales of turbulent motion to the small scales, which is characteristic of three-dimensional turbulence. This demonstrates transition from the quasi-two-dimensional turbulence within the surface region to the three-dimensional turbulence at large depths from the free surface. However, a more precise definition of the behavior of this two-dimensional region awaits future work.

V. INTERSCALE ENERGY TRANSFER AT FREE SURFACE

Energy transfer between the various length scales is the principal physical process influencing the evolution of the

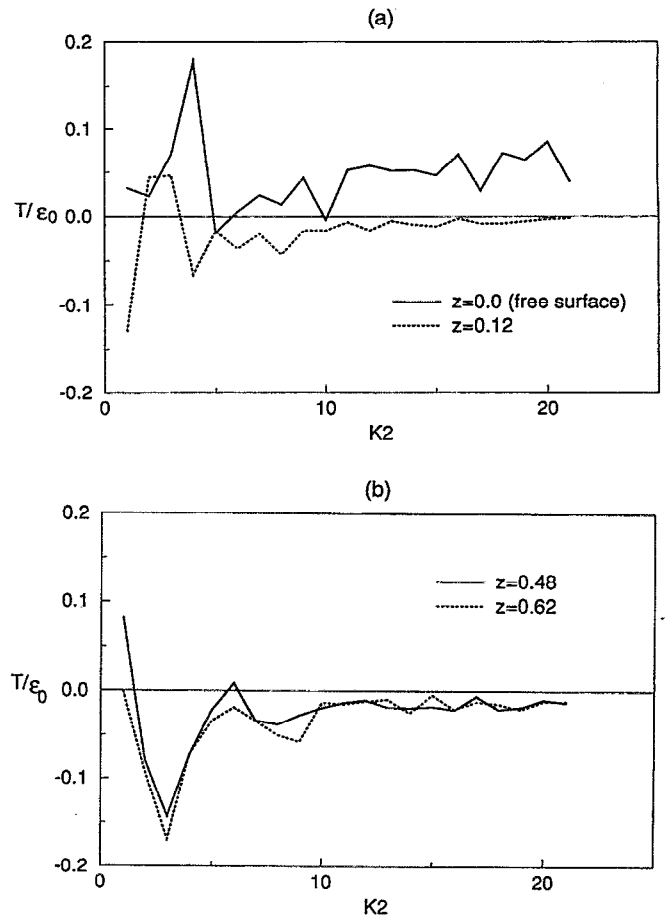

FIG. 14. Kinetic energy transfer spectra in horizontal planes at various depth below the free surface. The value of energy transfer is scaled by the plane averaged value of viscous dissipation rate.

turbulent flow field. The characteristics of free-surface turbulence, i.e., vortex generation, merging and pairing, upwelling, etc., are closely related to the energy transferred between different scales. While these processes in physical space were discussed previously, it is interesting to examine the energy transfer in wave space. The topic of interscale energy transfer in turbulent flows has been recently studied by Domaradzki and Rogallo,[37] Domaradzki,[38] Smyth,[39] Domaradzki *et al.*,[40,41] and Maltrud and Vallis.[42] In these studies, the triad interactions were investigated mainly for the purpose of examining the subgrid-scale models (SGS) in large-eddy simulations (LES). Our purpose is similar and, in the present study, is to study the behavior of the turbulence kinetic energy on the free surface as a function of wave number. This function will reveal the energy flux crossing a given wave number. We adopt a method used in study of the backscatter in SGS models for LES (Piomelli *et al.*[43]). A cutoff filter

$$\hat{G}_i(k_i)=\begin{cases}1 & \text{for } k_i\leqslant k_{ci},\\ 0 & \text{otherwise,}\end{cases} \tag{10}$$

where $\hat{G}_i$ is the Fourier coefficient of the filter function in the ith direction, k_{ci} is the cutoff wave number in the ith direc-

Copyright ©2001. All Rights Reserved.

tion, is applied onto the velocity fields obtained from the direct numerical simulation (DNS) of the Navier–Stokes equations. The velocity field is divided into resolved region ($k_i \leqslant k_{ci}$) and an unresolved region ($k_i > k_{ci}$). The transport equation for the resolved energy $\bar{q}=\bar{u}_i\bar{u}_i$ can be written as [the bars denoting application of the filter in Eq. (10)]

$$\frac{\partial \bar{q}}{\partial t}+\frac{\partial \bar{q}\bar{u}_j}{\partial x_j}=\frac{\partial}{\partial x_j}\left(-2\bar{p}\bar{u}_j-2\bar{u}_i\tau_{ij}+\frac{1}{\mathrm{Re}}\frac{\partial \bar{q}}{\partial x_j}\right)$$
$$-\frac{2}{\mathrm{Re}}\frac{\partial \bar{u}_i}{\partial x_j}\frac{\partial \bar{u}_i}{\partial x_j}+2\tau_{ij}\bar{S}_{ij}, \qquad (11)$$

where $\tau_{ij}=\overline{u_iu_j}-\bar{u}_i\bar{u}_j$ is called the SGS stress and $\bar{S}_{ij}=(1/2)(\partial\bar{u}_i/\partial x_j)$ is the large scale rate-of-strain tensor. The SGS dissipation $\epsilon_{\mathrm{sgs}}=\tau_{ij}\bar{S}_{ij}$ represents the energy transfer between resolved and unresolved scales. If it is negative, the unresolved scales remove energy from the resolved ones which is called forward scatter; if it is positive, they release energy to the resolved scales which is conventionally called backscatter. The backward and forward scatter components of ϵ_{sgs}, respectively denoted by ϵ_+ and ϵ_-, are defined by

$$\epsilon_+=\tfrac{1}{2}(\epsilon_{\mathrm{sgs}}+|\epsilon_{\mathrm{sgs}}|); \quad \epsilon_-=\tfrac{1}{2}(\epsilon_{\mathrm{sgs}}-|\epsilon_{\mathrm{sgs}}|), \qquad (12)$$

respectively. By changing the cutoff wave number in the filter, one can get the energy transfer cross-different wave numbers. Therefore, ϵ_{sgs}, ϵ_+, and ϵ_- are functions of cutoff wave number k_{ci}.

The cutoff filter, Eq. (10), involves two cutoff wave numbers, k_{c1} and k_{c2}, for streamwise and spanwise direction, respectively. Due to the fact that turbulence in channel flow is not exactly isotropic in the horizontal planes, the natural scale parameter, $k_c=\sqrt{k_{c1}^2+k_{c2}^2}$, which defines a circular shell in wave space, as is used in isotropic flows, does not exist. Here we adopt a scheme used by Domaradzki *et al.*,[38] where the resolved scales are identified with modes belonging to the rectangular region determined by $|k_1| \leqslant k_{c1}$ and $|k_2| \leqslant k_{c2}$. Conventionally, the two cutoffs, k_{c1} and k_{c2} are chosen in such a way that keeps the number of resolved Fourier modes in both directions the same, i.e., the resolved region is determined by

$$|k_1| \leqslant \frac{2\pi n_c}{L_1} \quad \text{and} \quad |k_2| \leqslant \frac{2\pi n_c}{L_2} \qquad (13)$$

in which n_c becomes the single parameter defining the cutoff scale. This approach takes into account the difference in scales in the x_1 and x_2 directions, by assuming that L_1 and L_2 are roughly proportional to them. (This works well if the simulation is done properly since then the streamwise and spanwise extent of the domain is made roughly proportional to the macroscales.)

The energy transfer between the resolved and unresolved scales is usually discussed in the context of a physical space representation, which does not provide information about its scale dependence. Here we present, in Fig. 15, the plane-averaged value of ϵ_{sgs}, ϵ_+, and ϵ_- at free surface, as functions of cutoff n_c. In other words, ϵ_{sgs} is the rate of energy transferred per unit mass by all modes in the region defined by Eq. (13) to modes which are outside that region. The values are normalized by the plane-averaged absolute value

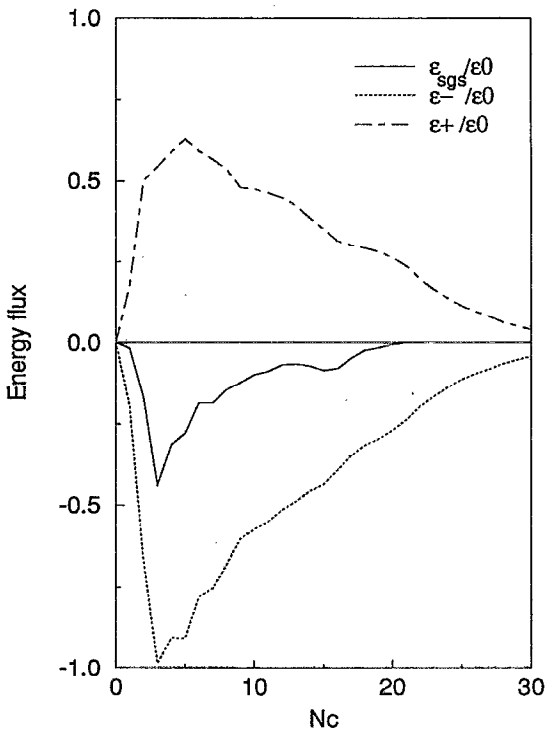

FIG. 15. Energy transfer as function of cutoff parameter, at the free surface.

of the viscous dissipation $\epsilon_0=(2/\mathrm{Re})S_{ij}S_{ij}$. This figure reveals some general features of the spectral energy transfer. In the low wave-number region, while the forward transfer dominates, as expected, the backward transfer is also quite significant. At high wave numbers, while both forward and backward transfer decrease in magnitude, they become equally important. This makes the net energy transfer between resolved and unresolved scales approaching zero as the cutoff wave number increases. At $n_c=0$, energy transfers are zero. This is due to the free surface boundary conditions. The peak values, i.e., the largest inverse and normal energy transfers, occur at about $n_c=5\sim6$. In physical space, this corresponds to the length scales of about 50~90 wall units. Recalling that the size of the whole free surface is about 1000×500 in wall units, these scales simply correspond to the large structures, such as vortices and upwellings. This point can be confirmed by comparing the ϵ_{sgs} distribution in physical space as shown in Fig. 16 and the flow pattern plots, as shown in Fig. 17.

Figure 16 shows the subgrid-scale energy transfer, ϵ_{sgs}, in the physical space representation at the free surface for three different cutoffs, viz. $n_c=6$, 12, and 19. Regions of the forward transfer (darker gray) and the inverse transfer (lighter gray) are clearly visible. It can be seen that the higher spectral cutoff wave number results in the presence of smaller scales in physical space. It can also be observed that forward and inverse transfer regions are roughly in balance, although the averaged net transfer is forward (negative). This is in agreement with the results of Piomelli *et al.*[41] who found that about 50% were characterized by the reverse energy transfer. In Fig. 17, we visualize the flow pattern at the

Copyright ©2001. All Rights Reserved.

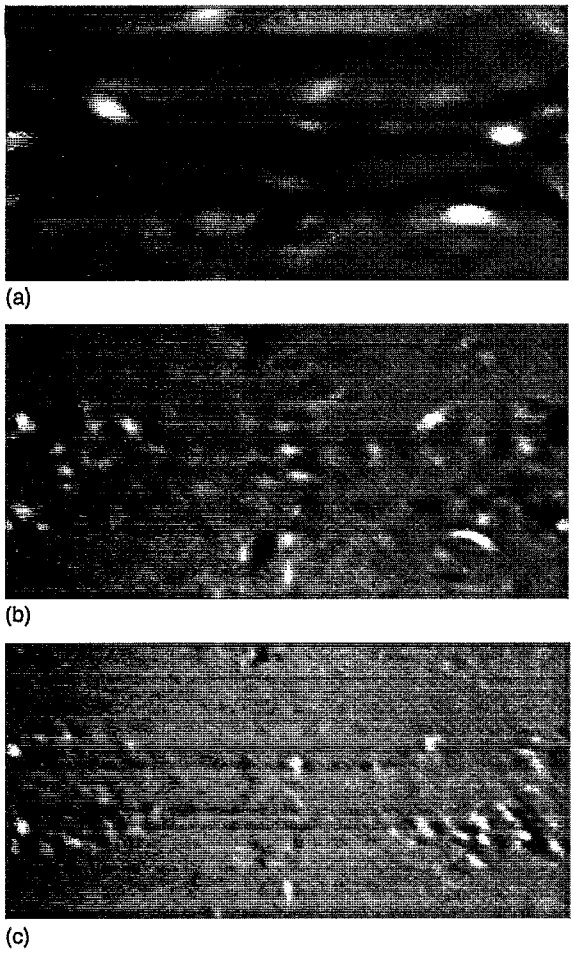

FIG. 16. The energy transfer in the physical space representation at the free surface: (a)=6; (b)=12; (c)=19. The light gray represents positive values (backward scatter) and the darker gray represents negative values (forward scatter). The velocity field is the same as that for plotting Fig. 15.

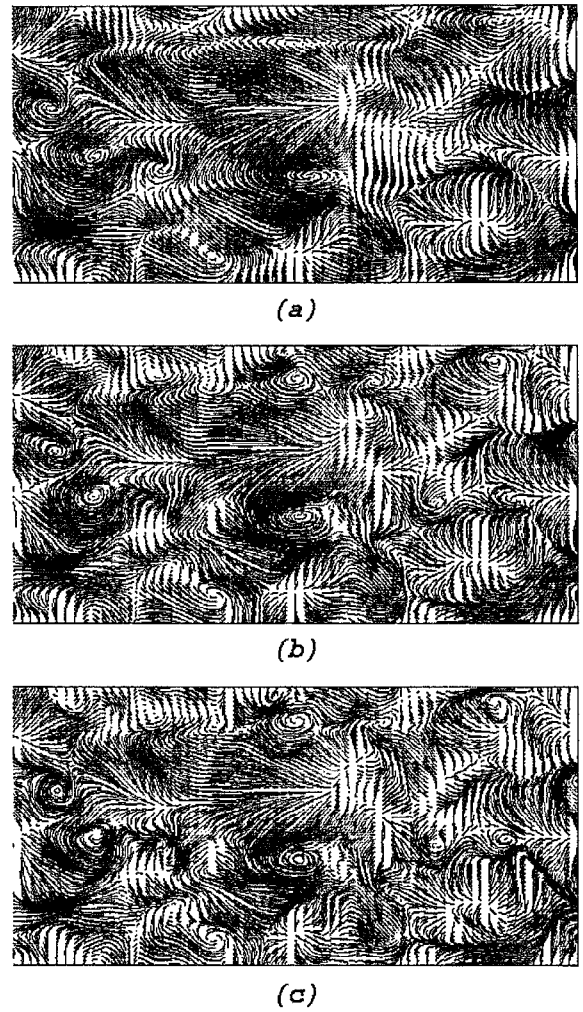

FIG. 17. Instantaneous streamlines visualized by filtered and unfiltered velocity field at the free surface: (a) filtered at=6; (b) filtered at=10; (c) unfiltered. The velocity field is the same as that for plotting Figs. 15 and 16.

free surface for the cases considered in Fig. 16 by plotting the instantaneous streamlines. Figures 17(a) and 17(b) are plotted with the filtered velocity fields with cutoff $n_c=5$ and $n_c=10$ respectively. Figure 17(c) is the unfiltered velocity field. It is easy to see that, with $n_c=5$, the signature of the large structures, i.e., vortices and upwellings, still remain in the flow, as shown by Fig. 17(a). One can further see that Fig. 17(b) is almost identical to Fig. 17(c) except for some small scales. By comparing Fig. 16(a) with Fig. 17(a), though we do not superimpose them, one finds that strong forward energy transfer occurs at the outskirt of the vortices and the strong reverse energy transfers are mostly in the regions with upwellings. Also, the vortices have at their core regions with weak energy transfer. This means that the energy contained in the vortices is conserved, to be expected since an important characteristic of the vortices, also observed in experiments, is their persistence.

VI. CONCLUSIONS

The direct numerical simulations indicate, as do experiments in a subsequent paper by Gupta *et al.*,[25] that the main structures that occur at unsheared free surface close to regions of turbulence generation, are upwellings which arise from impingement of large coherent structures such as bursts on the surface. Related to these are downdrafts which form in regions between upwellings where the flow that moves outward from adjacent upwellings impinge. The third structure which often occurs in the region of stagnation lines associated with the downdrafts are vortices (or more correctly spiral eddies) that appear to form in the regions where the stagnation lines are highly bent forming regions of high shear. These vortices originate due to the reconnection of the surface-parallel vorticity, carried by upwellings. Their presence is also detected in experiments. Besides these qualitative features, the energy spectra of turbulence at the free-surface exhibits two distinct ranges, viz. $k^{-5/3}$ and $k^{-3.5}$, which is the characteristic of two-dimensional turbulence. Gupta *et al.*[25] also obtained these characteristics in their experiments thus increasing confidence in the direct simulations presented here. The kinetic energy transfer function also provides the evidence of the existence of a quasi-two-dimensional region and the transition from two-dimensional to three-dimensional regions.

When such structures are allowed to decay by removing

Copyright ©2001. All Rights Reserved.

he source of turbulence generation, i.e., by changing the no-slip boundary condition on the bottom wall to a free-slip boundary condition, the upwellings and downdrafts, which cause the anisotropy near the free surface, start to disappear. The predominant patterns left on the free surface become the long-lived attached vortices. These vortices tend to pair, merge, and decay slowly. Examinations of the invariants of the anisotropy tensor suggest the transition from three-dimensional flow to two-dimensional flow at both the free surface and the free-slip wall (changed from a no-slip condition at the start of the decay phase). If one examines distributions of enstrophy and energy spectra within a region close to the free surface, the behavior also suggests an evolution that is essentially characteristic of decaying two-dimensional turbulence. Reverse energy transfer from small scales to large scales, associated with an increase of the integral scales and Taylor microscales, which is a feature of freely decaying two-dimensional turbulence, is evident in the free surface region. The interscale energy transfer was also investigated by calculating backward and forward scatter with a method used in SGS models for LES. The strongest turbulence activity occurs in the regions of upwellings and vortices where the energy transfers (both forward and backward) reach their peak value. The correlation between the forward–backward scatter and the flow pattern shows that strong forward energy transfer occurs at the outskirt of the vortices where the shear is high and strong backward transfer mostly in the regions with upwellings. The weak energy transfer observed in the vortex cores is consistent with the long-lived, persistent nature of these attached vortices.

It is possible that computational models for free-surface turbulence could be based on such structural considerations. Structural models, e.g., based on hairpin vortices, have had some success in modeling wall turbulence, and the quasi-two-dimensionality of free-surface turbulence offers simplifications that still need to be fully explored from a modeling view point.

The parameters governing the distance normal to the free surface over which quasi-two-dimensional behavior is seen has still to be explored, as do the parameter that governs the growth of this region in a decaying simulation, which might be of some practical interest. This study, therefore, identifies the qualitative features of the phenomena but does not as yet phrase, in quantitative terms, a prediction of the surface-normal distance over which two-dimensionality applies. To clarify these aspects, further simulations and experiments are necessary.

ACKNOWLEDGMENTS

We gratefully acknowledge the financial support for this research provided under ONR Grant (No. 0014-92-J-1077). This work is also related to a contract from DOE (DE-FG03-85ER13314) which was responsible for initiating much of the original developments with regard to free-surface direct simulations. We also acknowledge with gratitude the National Energy Research Supercomputer Center (NERSC), the San Diego Supercomputer Center (SDSC), and the National Center for Supercomputing Applications (NCSA) for computer resources.

[1] S. Komori, H. Ueda, F. Ogino, and T. Mizushina, "Turbulence structure and transport mechanism at the free surface in open channel flow," Int. J. Heat Mass Transfer **25**, 513 (1982).
[2] M. Rashidi and S. Banerjee, "Turbulence structure in free-surface channel flows," Phys. Fluids **31**, 2491 (1988).
[3] M. Rashidi and S. Banerjee, "The effect of boundary conditions and shear rate on streak formation and breakdown in turbulent channel flows," Phys. Fluids A **2**, 1827 (1990).
[4] M. Rashidi and S. Banerjee, "Streak characteristics and behavior near wall and interface in open channel flows," J. Fluid Eng. (ASME) **112**, 164 (1990).
[5] S. Banerjee, "Turbulence structure and transport mechanisms at interfaces," *Proceedings of the Ninth International Heat Transfer Conference,* Keynote Lecture (Hemisphere, New York, 1990), Vol. 1, pp. 395–418.
[6] K. Lam and S. Banerjee, "Investigation of turbulent flow bounded by a wall and a free surface," *Proceedings of the Annual ASME Meeting,* Invited Paper, Chicago (American Society of Mechanical Engineers, New York, 1988), pp. 72–79.
[7] K. Lam and S. Banerjee, "On condition of streak formation in a bounded turbulent flow," Phys. Fluids A **4**, 306 (1992).
[8] S. Komori, R. Nagaosa, Y. Murakami, S. Chiba, K. Ishii, and K. Kuwahara, "Direct numerical simulation of three-dimensional open channel flow with zero-shear gas–liquid interface," Phys. Fluids A **5**, 115 (1993).
[9] R. A. Handler, T. F. Swean, Jr., R. I. Leighton, and J. D. Swearingen, "Length scales and energy balance for turbulence near a free surface," AIAA J. **31**, 1998 (1993).
[10] S. Banerjee, "Upwellings, downdrafts, and whirlpools: dominant structures in free surface turbulence," Appl. Mech. Rev. **47**, Part 2, 166 (1994).
[11] S. Komori, R. Nagaosa, and Y. Murakami, "Turbulence structures and mass transfer across a sheared air–water interface in a wind-driven turbulence," J. Fluid Mech. **249**, 161 (1993).
[12] T. Sarpkaya and P. Suthon, "Interaction of a vortex couple with a free surface," Exp. Fluids **11**, 205 (1991).
[13] T. F. Swean, Jr. and A. N. Beris, "Dynamics of free-surface flows with surfactants," (Proceedings of the Twelfth US National Congress of Applied Mechanics), Appl. Mech. Rev. **47**, Part 2, 173 (1994).
[14] J. Kim, P. Moin, and R. Moser, "Turbulence statistics in a fully developed channel flow at low Reynolds number," J. Fluid Mech. **177**, 133 (1987).
[15] K. Lam, "Numerical investigation of turbulent flow bounded by a wall and a free-slip surface," Ph.D. thesis, University of California at Santa Barbara, Santa Barbara, CA, 1989.
[16] A. Perry and M. S. Chong, "A description of eddying motions and flow patterns using critical point concepts," Annu. Rev. Fluid Mech. **19**, 125 (1987).
[17] G. S. Hirschberg, "Direkte simulation der turbulenten Taylor–Couette Strömung und der ebenen Kanalströmung," Ph.D. dissertation, ETH, Zrich, Switzerland, 1992.
[18] M. S. Chong, A. Perry, and B. J. Cantwell, "A general classification of three-dimensional flow fields," Phys. Fluids A **2**, 765 (1990).
[19] J. C. R. Hunt, A. A. Wray, and P. Moin, "Eddies, streams and convergence zones in turbulent flow," Proceedings of the 1988 Summer Program, NASA/Sanford Center for Turbulence Research, 1988, pp. 193–208.
[20] J. C. McWilliams, "The emergence of isolated coherent vortices in turbulent flow," J. Fluid Mech. **146**, 21 (1984).
[21] N. D. Sandham and L. Keiser, "The late stages of transition to turbulence in channel flow," J. Fluid Mech. **245**, 319 (1992).
[22] M. E. Brachet, "Direct simulation of three-dimensional turbulence in the Taylor–Green vortex," Fluid Dyn. Res. **8**, 1 (1991).
[23] S. Douady, Y. Couder, and M. E. Brachet, "Direct observation of the intermittency of intense vorticity filaments in turbulence," Phys. Rev. Lett. **67**, 983 (1991).
[24] S. Robinson, "Coherent motions in the turbulent boundary layer," Annu. Rev. Fluid Mech. **23**, 601 (1991).
[25] R. Gupta, S. Kumar, and S. Banerjee, "Characteristics of attached vortices in free surface channel flows," presented at 12th U.S. National Congress of Applied Mechanics, Seattle, Washington, 27 June–1 July (also submitted to Phys. Fluids).
[26] D. G. Dommermuth, "The laminar interactions of a pair of vortex tubes with a free surface," J. Fluid Mech. **246**, 91 (1993).
[27] E. Rood, "Myths, math, and physics of free-surface vorticity," Appl. Mech. Rev. **47**, Part 2, S152 (1994).
[28] J. C. McWilliams, "A demonstration of the suppression of turbulent cascades by coherent vortices in two-dimensional turbulence," Phys. Fluids A **2**, 547 (1990).

Copyright ©2001. All Rights Reserved.

[29]M. E. Brachet, M. Meneguzzi, H. Politano, and P. L. Sulem, "The dynamics of freely decaying two-dimensional turbulence," J. Fluid Mech. **194**, 333 (1988).
[30]P. Santangelo, R. Benzi, and B. Legras, "The generation of vortices in high resolution, two-dimensional decaying turbulence and the influence of initial conditions on the breaking of self-similarity," Phys. Fluids A **1**, 1027 (1989).
[31]R. H. Kraichnan, "Inertial ranges in two-dimensional turbulence," Phys. Fluids **10**, 1417 (1967).
[32]G. K. Batchelor, "Computation of the energy spectrum in homogeneous two-dimensional turbulence," Phys. Fluids, Suppl. 2, 233 (1969).
[33]S. Narimousa, T. Maxworthy, and G. R. Spedding, "Experiments on forced, quasi-two-dimensional turbulence at upwelling fronts," *Turbulence and Coherent Structures* (Kluwer Academic, New York, 1989).
[34]J. C. R. Hunt and J. M. R. Graham, "Free stream turbulence near plane boundaries," J. Fluid Mech. **84**, 209 (1978).
[35]J. L. Lumley, "Computational modeling of turbulence flows," Adv. Appl. Mech. **18**, 123 (1978).
[36]G. F. Smith, "On isotropic functions of symmetric tensors, skew-symmetric tensors and vectors," Int. J. Eng. Sci. **9**, 899 (1971).
[37]J. A. Domaradzki and R. S. Rogallo, "Local energy transfer and nonlocal interactions in homogeneous, isotropic turbulence," Phys. Fluids A **2**, 413 (1990).
[38]J. A. Domaradzki, "Nonlocal triad interactions and the dissipation range of isotropic turbulence," Phys. Fluids A **4**, 2037 (1992).
[39]W. D. Smyth, "Spectral transfers in two-dimensional anisotropic flow," Phys. Fluids A **4**, 340 (1992).
[40]J. A. Domaradzki, W. Liu, and M. E. Brachet, "An analysis of subgrid-scale interactions in numerically simulated isotropic turbulence," Phys. Fluids A **5**, 1747 (1993).
[41]J. A. Domaradzki, W. Liu, C. Hertel, and L. Kleiser, "Energy transfer in numerically simulated wall-bounded turbulence flows," Phys. Fluids **6**, 1583 (1994).
[42]M. E. Maltrud and G. K. Vallis, "Energy and enstrophy transfer in numerical simulations of two-dimensional turbulence," Phys. Fluids **5**, 1760 (1993).
[43]U. Piomelli, W. H. Cabot, P. Moin, and S. Lee, "Subgrid-scale backscatter in turbulent transitional flows," Phys. Fluids A **3**, 1766 (1991).

Copyright ©2001. All Rights Reserved.